iScience

Article

Programmed cell senescence is required for sensory organ development in *Drosophila*

Graphical abstract

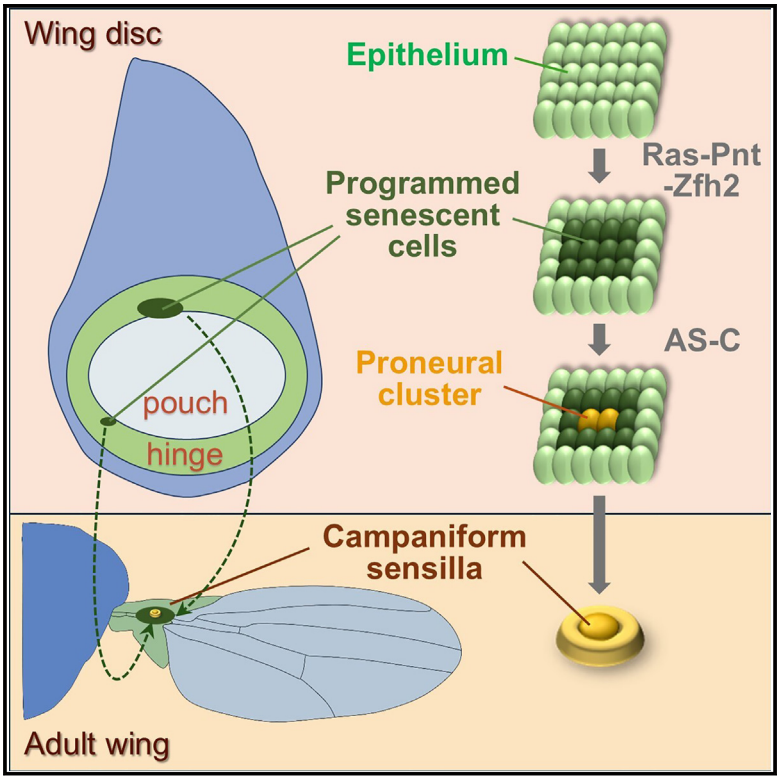

Authors

Yiran Zang, Masanari Yoshimoto, Tatsushi Igaki

Correspondence

igaki.tatsushi.4s@kyoto-u.ac.jp

In brief

Molecular biology; Cell biology; Developmental biology

Highlights

- Developmentally programmed cellular senescence occurs in *Drosophila* wing discs
- Programmed senescent cells exhibit hallmarks of cellular senescence
- Programmed cell senescence is caused by the Ras-Pointed-Zfh2 pathway
- Programmed cell senescence is required for the formation of a specific sensory organ

Zang et al., 2025, iScience *28*, 112048
March 21, 2025
https://doi.org/10.1016/j.isci.2025.112048

CellPress

iScience

CellPress
OPEN ACCESS

Article

Programmed cell senescence is required for sensory organ development in *Drosophila*

Yiran Zang,[1] Masanari Yoshimoto,[1] and Tatsushi Igaki[1,2,*]
[1]Laboratory of Genetics, Graduate School of Biostudies, Kyoto University, Yoshida-Konoecho, Sakyo-ku, Kyoto 606-8501, Japan
[2]Lead contact
*Correspondence: igaki.tatsushi.4s@kyoto-u.ac.jp
https://doi.org/10.1016/j.isci.2025.112048

SUMMARY

Cellular senescence is an irreversible cell-cycle arrest often associated with cancer and aging, yet its physiological role remains elusive. Here, we show developmentally programmed cellular senescence occurs in *Drosophila* imaginal epithelium. In developing wing discs, two clusters of cells exhibit hallmarks of cellular senescence such as elevated senescence-associated β-galactosidase activity, cell-cycle arrest, heterochromatinization, upregulation of a cyclin-dependent kinase (CDK) inhibitor Dacapo, cellular hypertrophy, Ras signaling activation, and upregulation of an inflammatory cytokine unpaired3, a possible component of the senescence-associated secretory phenotype. Blocking programmed cell senescence by inhibiting Ras signaling or its downstream transcription factor Pointed (Pnt) results in loss of sensory organ campaniform sensilla. Ras-Pnt signaling causes programmed cell senescence through a transcription factor Zfh2, thereby contributing to campaniform sensilla formation via the *achaete-scute* complex. Our observations uncover the evolutionary conservation of programmed cell senescence in invertebrates, which is required for the induction of the proper number of sensory organs.

INTRODUCTION

Cellular senescence, a state of irreversible cell-cycle arrest, often occurs under stressed conditions such as tumorigenesis, aging, and tissue damage.[1,2] Thus, until recent years, most studies on cellular senescence have focused on its roles and mechanisms under pathological environments and revealed that it plays beneficial roles in promoting tumor suppression and tissue repair, while having detrimental roles in accelerating tumorigenesis and aging.[3] In these events, cellular senescence is induced via ectopic elevation of oncogene activity, oxidative stress, DNA damage, and chronic inflammation caused by a variety of pathologies or gene mutations.[4–8]

Cellular senescence is often characterized by elevation of senescence-associated β-galactosidase (SA-β-gal) activity, upregulation of cyclin-dependent kinase (CDK) inhibitors, accumulation of heterochromatin foci, elevation of DNA damage response, and enlarged cell size.[2,9] Intriguingly, using these markers, studies in vertebrate models have identified senescent cells during normal embryonic development. In mouse or chick embryos, senescent cells can be found in regressing mesonephric tubules, inner ears, apical ectodermal ridge (AER), interdigital webs, and neural tubes.[10,11] Abrogating cellular senescence in mouse embryos by deleting the CDK inhibitor *p21* gene causes patterning defects in related tissues such as Wolffian duct and limbs, suggesting the role of developmentally programmed cell senescence in tissue remodeling.[10,11] In addition, programmed cell senescence was found in the hair follicles of newborn naked mole rats, which is suggested to be the reason why naked mole rats are hairless.[12] Moreover, senescence-like cells with elevated SA-β-gal activity were observed in quail embryos, and transforming growth factor β (TGFβ)-dependent senescent cells were found in axolotl and Xenopus embryos.[13,14] These observations suggest that developmentally programmed cell senescence commonly exists across vertebrates. However, the mechanisms and physiological roles of programmed cell senescence are still largely unknown.

Drosophila provides a powerful genetic model to study the physiological roles and mechanisms of biological phenomena during normal development. A previous study has shown that, in developing *Drosophila* imaginal epithelia, ectopic activation of the Ras oncogene with simultaneous mitochondrial defects causes cellular senescence that exhibits all markers of senescent cells described above.[15] This suggests that senescent cells in *Drosophila* share a similar mechanism with those in vertebrate animals under pathological environment and leads us to inquire whether programmed cell senescence also exists in *Drosophila* during normal development.

Here, we find that programmed cell senescence indeed occurs in developing invertebrate tissues, the wing imaginal discs in *Drosophila* larva. Furthermore, abrogating cellular senescence in these tissues results in loss of sensory organ campaniform sensilla, a special type of mechanoreceptor located on the dorsal and ventral radius of adult wings. Our data suggest that developmentally programmed senescence pathway is integrated with the campaniform sensilla development through the

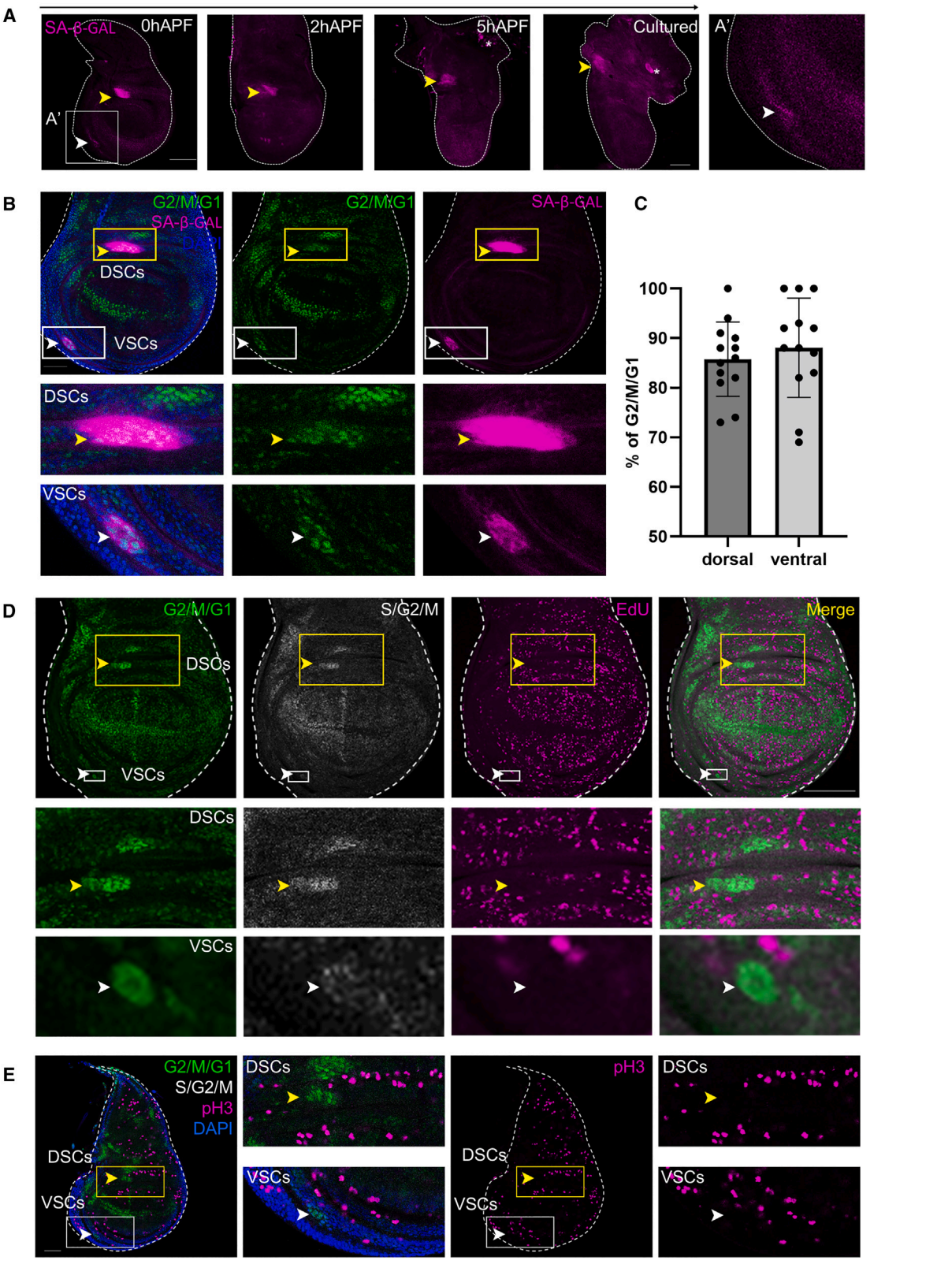

(legend on next page)

Ras-Pnt pathway in *Drosophila*. We further identified a new senescence regulator *zfh2* that mediates both programmed cell senescence and oncogene-induced senescence.

RESULTS

Programmed cell senescence occurs in developing *Drosophila* wing disc

To investigate whether programmed cell senescence occurs during *Drosophila* development, we performed SA-β-gal staining in a variety of tissues in 3rd instar larvae. An intense SA-β-gal signal at pH6.0 was reproducibly observed around the center of the wing imaginal discs (Figure S1A, yellow arrowheads). A cluster of cells with elevated SA-β-gal activity began to appear at the middle L3 (ML3) stage, and the signal intensity increased as larvae grew into late L3 (LL3) (Figures 1A and S1A). Notably, no β-gal activity was observed at pH7.5 (Figure S1A), indicating that the elevated SA-β-gal signal was not simply due to increased β-gal expression but specifically due to senescence-associated β-gal activation. We further analyzed SA-β-gal activity in the wing discs at pupal stage using a more sensitive fluoresce probe SPiDER-βGal at pH6.0.[16] The morphology of the wing disc changed dramatically after puparium formation (APF), but the SA-β-gal activity still existed even at 5-h APF (Figure 1A, yellow arrowheads). As later stage, wing discs recruit many hemocytes, which are strongly stained with SPiDER-βGal or SA-β-gal and thus hampers our analysis. We performed *ex vivo* culture of L3 wing discs in a hemocyte-free medium for 24 h and found that the cluster of cells with elevated SA-β-gal activity still existed in the wing disc at pre-pupal phase 3 (PP3) (∼9 h APF) (Figure 1A).[17,18] We also noticed that there existed a smaller cluster of cells with elevated SA-β-gal activity at the ventral hinge of the wing disc (Figures 1A and 1A′, white arrowheads). Hereafter, we call these reproducibly observed large and small clusters of cells with elevated SA-β-gal activity as dorsal senescent cells (DSCs; yellow arrowheads) and ventral senescent cells (VSCs; white arrowheads), respectively. Other tissues such as leg discs, haltere discs, and the brain, but not salivary gland, fat bodies, and eye discs (except for the hemocytes attached to the discs), showed some SA-β-gal activities (Figure S1B). We focused our analyses on the SA-β-gal-positive clusters in wing discs, as they exhibit highly reproducible, intense SA-β-gal staining with low background.

One important aspect of cellular senescence is cell-cycle arrest. Consequently, we first analyzed cell-cycle phases of DSCs and VSCs using the cell-cycle monitoring probe fly FUCCI.[19] We found that 85.8% of DSCs (yellow arrowheads) were GFP (G2/M/G1)-positive and 88.0% of VSCs (white arrowheads) were GFP (G2/M/G1)-positive (Figures 1B and 1C). Both DSCs and VSCs exhibited GFP (G2/M/G1) and RFP (S/G2/M) signals (Figures 1D and 1E), suggesting that they were at G2 or M phase. In addition, the lack of EdU staining, a widely used marker for S phase, in DSCs and VSCs indicated that those cells are not in S phase (Figure 1D). Moreover, phosphohistone H3 (pH3) staining, which labels cells in M phase, failed to stain DSCs and VSCs, indicating that they are arrested in G2 phase (Figure 1E, yellow and white arrowheads). These data indicate that a major population of SA-β-gal-positive cell clusters in the wing discs undergo cell-cycle arrest in G2 phase.

To verify whether DSCs and VSCs are indeed undergoing cellular senescence, we further examined other hallmarks of senescence. First, upregulation of a CDK inhibitor Dacapo (Dap, a p21 homologue), an important feature of cellular senescence, was observed in these cell clusters as visualized by anti-Dap immunostaining (Figure 2A, quantified in Figure 2B). This suggests that besides G2 arrest, at least small populations of SA-β-gal-positive cell clusters undergo G1 arrest. Second, trimethylation of histone H3-K9, which is associated with the senescence-associated heterochromatin foci, was elevated in DSCs and VSCs (Figure 2C, quantified in Figures 2D and 2E). Third, oxidative stress, which is often associated with senescent cells, was increased in DSCs and VSCs, as visualized by the gstD-GFP probe (Figure S2A). Fourth, both DSCs and VSCs underwent cellular hypertrophy, another hallmark of senescent cells (Figures 2F and 2G). These data suggest that two clusters of cells, DSCs and VSCs, in *Drosophila* wing discs undergo developmentally programmed cell senescence.

We further explored whether senescence-associated secretory phenotype (SASP) is induced in the senescent clusters. We did not detect expression of *unpaired* (*upd*, an interleukin-6 [*IL-6*] homologue) or *matrix metalloproteinase 1* (*mmp1*), typical SASP factors in mammals, in the wing disc (Figures S2C–S2E). However, intriguingly, an *IL-6* homologue *unpaired3* (*upd3*), which activates *Drosophila* JAK/STAT signaling, was significantly upregulated in DSCs and VSCs as visualized by the *upd3-gal4* reporter (Figure 2H). These data suggest that SASP may also be induced in programmed senescent cells in the wing discs.

Programmed cell senescence is required for proper development of sensory organ campaniform sensilla

We next investigated the upstream trigger of programmed cell senescence in the wing discs. Epidermal growth factor receptor [EGFR]-Ras signaling, a known trigger of cellular senescence in mammals, was upregulated in DSCs and VSCs, as visualized by the Ras signaling effector pERK staining, which was co-localized with the SA-β-gal staining (Figure 3A, quantified in Figure 3B). Elevation of EGFR signaling was also confirmed by downregulation of a transcription factor Capicua[20] (Figure S3A).

Figure 1. Two clusters of cells with elevated SA-β-gal activity and cell-cycle arrest appear in developing wing discs

(A) Wild-type wing discs were stained with SPiDER-βgal. Arrowheads indicate SA-β-gal-activated clusters. Asterisks represent hemocytes that attach to the wing disc. APF, after puparium formation.

(B and C) Wing discs expressing fly-FUCCI were stained with SPiDER-βgal (B), and percentage of G2/M/G1 cells (green) in SA-β-gal-activated clusters (magenta) was quantified in (C). Dorsal cells (n = 13), ventral cells (n = 13).

(D and E) Wing discs expressing fly-FUCCI were stained with EdU (D) or phosphohistone H3 (pH3) antibody (E). GFP-E2F1 represents G2/M/G1 phase (green), and mRFP-NLS-CycB represents S/G2/M phase (white). Yellow arrowheads indicate dorsal senescent cells (DSCs), whereas white arrowheads indicate ventral senescent cells (VSCs). Scale bars, 100 μm (A, D), 50 μm (B, E). See Table S1 for genotypes.

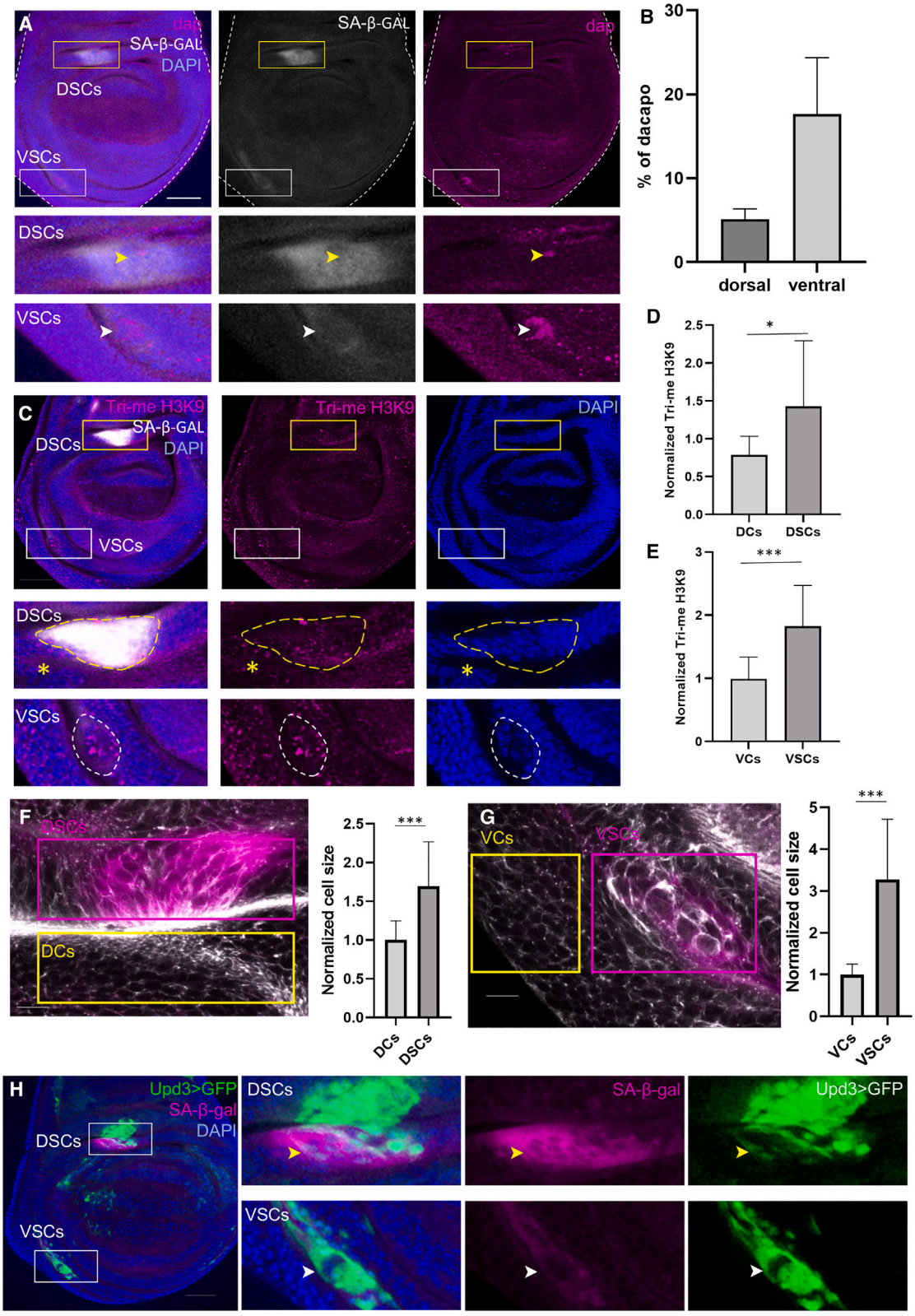

(legend on next page)

In addition, inhibition of Ras signaling by Ras^{N17}, a dominant-negative form of Ras, using the *ci*-Gal4 driver suppressed endogenous SA-β-gal activity (Figure 3C, quantified in Figure 3D). We further verified this by using the *ap-GAL4* driver and found that SA-β-gal activity is indeed suppressed by Ras^{N17} (Figure S3B, quantified in Figure S3C). These data suggest that Ras signaling acts as an upstream trigger of programmed cell senescence.

We next sought to identify the cell type of the clusters undergoing programmed cell senescence in the wing discs. The clusters of DSCs and VSCs are located at the anterior part of the wing disc near the anterior/posterior (A/P) boundary (Figure S3D, arrowheads), as assessed by *ci*-Gal4 that is expressed in the whole anterior compartment. Analysis with *nub*-GAL4, which drives gene expression in the wing pouch and a part of hinge, revealed that both DSCs and VSCs are located at the hinge region right next to the wing pouch (Figure S3E, arrowheads). Further analysis with DAPI staining, which visualizes the folding of the wing disc, showed that both DSCs and VSCs are located on the distal hinge (DH) (Figure 3E). Interestingly, these two locations, the regions of DSCs and VSCs, develop into the dorsal and ventral compartments of the adult wing hinge close to the wing blade, respectively: the regions called dorsal and ventral radiuses (Figure 3F). The dorsal and ventral radiuses possess sensory organs called campaniform sensilla, mechanoreceptors derived from proneural clusters in the wing disc (Figure 3G, arrows). Notably, although there are different types of campaniform sensilla, the campaniform sensilla on DSCs and VSCs commonly exhibit a specific feature denoted as circular, low-profile sensilla with a socket.[21] We further analyzed DSCs and VSCs in the wing disc and found that they were indeed co-localized with the proneural markers achaete (Ac) and scabrous (Sca) (Figures S3F and S3G). Strikingly, suppression of programmed cell senescence by blocking Ras signaling (Ras^{N17}) using the *ci*-Gal4 driver resulted in a significantly reduced number of campaniform sensilla on both dorsal and ventral radiuses (Figure 3H, quantified in Figure 3I). These data suggest that programmed cell senescence is required for proper development of the special type of campaniform sensilla at dorsal and ventral radiuses.

Programmed cell senescence is caused by Ras-induced *pnt* expression

We next examined how programmed cell senescence is induced in the wing disc. In mammals, Ras-induced cellular senescence is mediated by the ETS1/2 transcription factor.[22] *Drosophila* has an *ETS1/2* homologue *pointed* (*pnt*), which encodes two protein isoforms PntP1 and PntP2.[23,24] PntP1 is transcriptionally regulated by EGFR-Ras signaling and induces downstream genes that are required for development of photoreceptor neurons in eye imaginal discs.[25] We have found that PntP1 is a necessary and sufficient downstream effector of Ras-induced cellular senescence in the imaginal discs.[26] Notably, we found that PntP1 expression was induced in both DSCs and VSCs (Figure 4A). This upregulation of PntP1 was abolished when Ras-MAPK signaling was blocked by overexpression of Ras^{N17} or knockdown of MAPK *rolled* (*rl*) (Figures 4B and 4C), suggesting that PntP1 acts as a downstream effector of Ras-MAPK signaling in DSCs and VSCs. Crucially, knockdown of *Pnt* using the *ci*-Gal4 driver suppressed SA-β-Gal activity in these senescent cells (Figure 4D, quantified in Figure 4E). We further confirmed this result by using *ap-GAL4* and *pnt*-RNAi, which significantly suppressed SA-β-Gal activity in DSCs (Figure S4A, quantified in S4B). Furthermore, blocking Ras-MAPK signaling caused the emergence of cells at S and M phase in DSCs and VSCs, as visualized by EdU labeling and pH3 staining (Figures 4F, 4G, and 4J–4K; asterisks, quantified in 4H, 4I, 4L, and 4M). We also found by pH3 and EdU staining that cell-cycle arrest in DSCs and VSCs was significantly suppressed by overexpression of String (Stg), a downstream cell-cycle regulator of Ras signaling (Figures S4C and S4F, quantified in Figures S4D, S4E, S4G, and S4H). These data indicate that programmed cell senescence in the wing discs is caused by Ras-induced PntP1 expression.

Programmed cell senescence promotes campaniform sensilla development via pnt-AS-C-mediated proneural cluster formation

We next investigated how PntP1-mediated cellular senescence promotes development of campaniform sensilla. Consistent with our data that Pnt is required for the induction of programmed cell senescence, knockdown of *pnt* resulted in loss of campaniform sensilla in the adults (Figure 5A, quantified in Figure 5C). It is known that the basic helix-loop-helix transcriptional factor *achaete-scute* (*ac-sc*) complex (AS-C) plays an essential role in sensory organ development in *Drosophila*. However, whether Pnt regulates proneural clusters in campaniform sensilla has been unclear, as most studies have focused on sensory bristles and chordotonal organs.[27,28] Significantly, blocking programmed cell senescence by *pnt*-RNAi using the *ci*-Gal4 driver strongly suppressed Ac expression at the clusters of DSCs and VSCs (Figures 5C and 5D, quantified in 5G and 5H). Notably, Ac expression along the DV boundary, which become bristles in the adults, were unaffected by *pnt* knockdown (Figures 5C and 5D, asterisks). Furthermore, knockdown of *ac* and *sc* using the *nub-Gal4* abolished campaniform sensilla development at dorsal and

Figure 2. SA-β-gal-elevated cells undergo cellular senescence

(A and B) Wild-type wing discs were stained with SPiDER-βgal and anti-dacapo (A). Percentage of positive cells (magenta) in SA-β-gal-activated clusters (white) were quantified in (B). Dorsal cells (n = 8), ventral cells (n = 8).

(C–E) Wild-type wing discs were stained with SPiDER-βgal and anti-Histone H3 (trimethyl K9). Intensity of Tri-me H3K9 (magenta) was measured within each nucleus, marked by DAPI staining (blue), and normalized with corresponding DAPI intensity. Outlined areas indicate senescent cells, and asterisks indicate neighboring normal cells. Data were collected as mean ± SE; normal dorsal cells (DCs) (n = 12); DSCs (n = 12); normal ventral cells (VCs) (n = 12); VSCs (n = 12). Student's t test, $^{*}p < 0.05$, $^{***}p < 0.001$.

(F and G) Wild-type wing disc was stained with SPiDER-β-gal (magenta) and phalloidin (white). Cell size was analyzed with three biological replicates, measured with ImageJ and quantified as relative size to neighboring normal cells. Data were collected as mean ± SEs; normal dorsal cells (DC) (n = 97); DSCs (n = 97); normal ventral cells (VC) (n = 58); VSCs (n = 58). Student's t test, $^{***}p < 0.001$.

(H) Wing discs carrying *Upd3>GFP* were stained with SPiDER-βgal. Scale bars, 50 μm (A, C, H) or 10 μm (F). See Table S1 for genotypes.

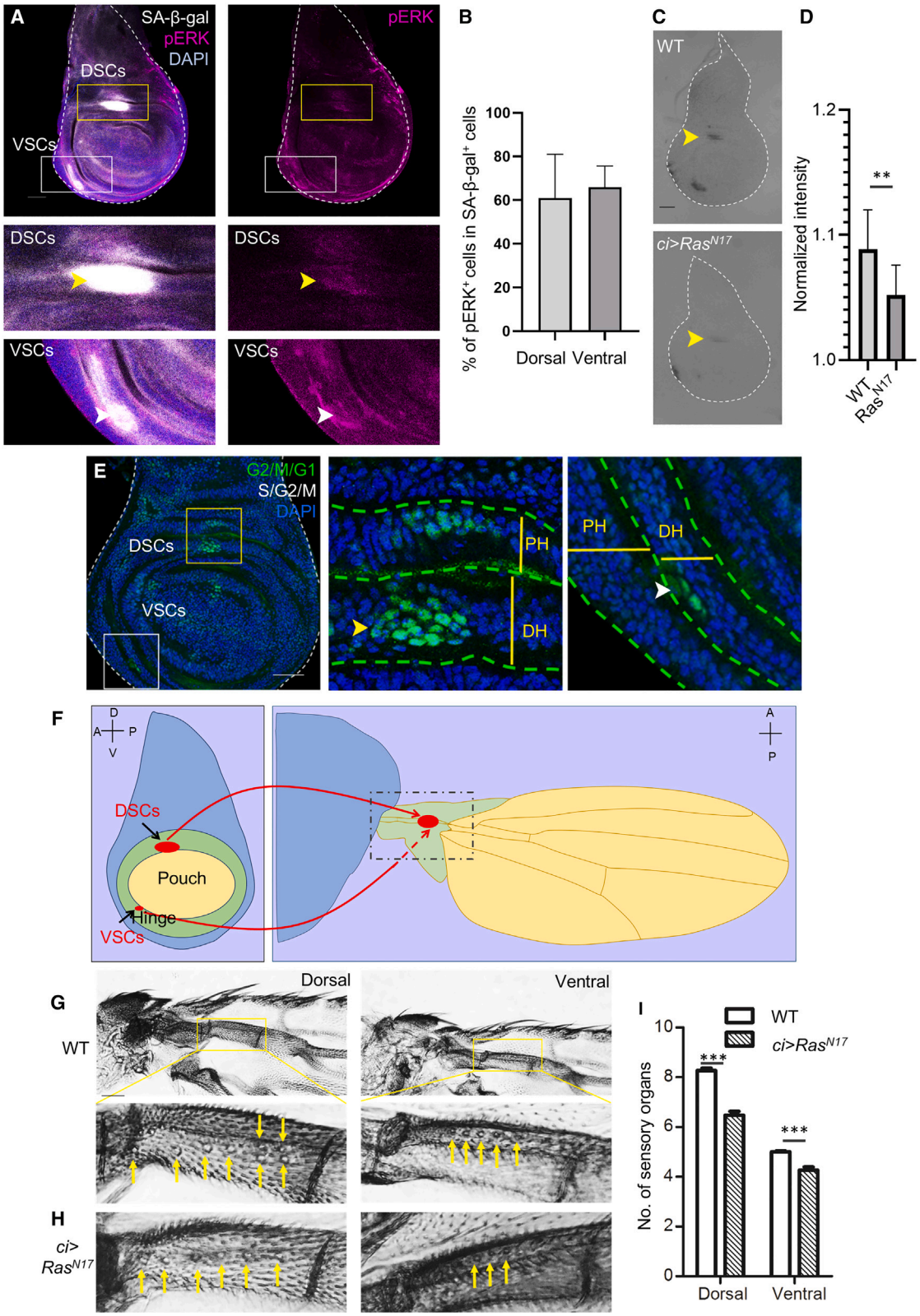

(legend on next page)

ventral radiuses of the adult hinge (Figure 5E, quantified in Figure 5I) without affecting SA-β-gal activity in the programmed senescent cells (Figure 5F, quantified in Figure 5J). These data indicate that AS-C acts downstream of Pnt, which has been suggested before[29]. Given that AS-C is generally required for the induction of sensory organs, Pnt-induced cellular senescence may be required for the formation of a special type of campaniform sensilla at dorsal and ventral radiuses of the hinge. These results suggest that programmed cell senescence contributes to the development of a special type of sensory organ in the wing hinge through Pnt-AS-C-mediated formation of proneural clusters.

Ras-Pnt-dependent programmed cell senescence is mediated by *zfh2*

To further confirm the role of programmed cell senescence in campaniform sensilla development, we searched for other genes that regulate programmed cell senescence in the wing disc. By performing an RNAi screening of genes abundantly expressed in the hinge region of the wing disc,[30] we found that knockdown of a transcription factor *Zn finger homeodomain 2* (*zfh2*) strongly blocked programmed cell senescence (Figure 6A, quantified in Figure 6C). We further confirmed this by using *ap-GAL4*, which showed a blockade of programmed cell senescence in dorsal cells (Figure S5A). Notably, *zfh2* is an ortholog of *AT-motif binding factor 1* (*ATBF1*), which is often mutated or deleted in various cancers and is decreased in Ras^{ACT}- and $Notch^{ACT}$-driven tumors in *Drosophila*,[31] suggesting that *zfh2* might act as a tumor suppressor by inducing cellular senescence. Indeed, loss of *zfh2* suppressed not only programmed cell senescence but also oncogene-induced senescence, as Ras^{V12}-induced SA-β-gal activity[15] was significantly reduced by *zfh2* knockdown (Figure 6B, quantified in Figure 6D). This suggests that the inhibition of programmed cell senescence by *zfh2* knockdown is not the result of abnormal hinge development but is due to blockage of senescence signaling. Indeed, the expression of *pnt-lacZ* in DSCs and VSCs was strongly downregulated by *zfh2* knockdown (Figure 6E). Furthermore, the development of campaniform sensilla was severely impaired by loss of *zfh2* (Figure 6F, quantified in Figure 6G). Together, these data suggest that *pnt*-dependent programmed cell senescence triggered by Ras signaling is mediated by *zfh2* and that programmed cell senescence plays an essential role in campaniform sensilla development (Figure 6H).

DISCUSSION

In this study, we report that two clusters of cells in *Drosophila* wing discs, both of which develop into campaniform sensilla on the adult hinge radiuses, undergo programmed cell senescence during larval and pupal development. Our data show that programmed cell senescence is a common developmental process conserved from invertebrates to vertebrates. A series of genetic data indicate that programmed cell senescence in the wing discs is integrated with development of a special type of campaniform sensilla via the Ras-Zfh2-Pnt-mediated signaling pathway. This is similar to the role of programmed cell senescence in mammals, which is also essential for normal tissue development.[10,11]

Programmed senescent cells in *Drosophila* exhibit many hallmarks of cellular senescence such as elevation of SA-β-gal activity, cell-cycle arrest, heterochromatinization, upregulation the p21 homolog *dacapo*, oxidative stress, cellular hypertrophy, Ras-ERK signaling activation, and elevation of a possible SASP factor, except for DNA damage response (data not shown), which is consistent with the programmed cell senescence in vertebrates.[10,11] In mouse embryos, ERK also regulates programmed cell senescence and thus AER patterning in a paracrine manner.[10] On the other hand, in amphibians, programmed cell senescence occurs independently of ERK signaling.[14] In *Drosophila* imaginal epithelium, pERK is detected not only in programmed senescent cells but also in non-senescent cells. These observations suggest that pERK plays a crucial role in some contexts but is not a necessary and sufficient factor for the induction of cellular senescence.

Although mammalian programmed senescent cells in AER are removed by apoptosis and macrophage-mediated clearance,[10] programmed senescent cells in *Drosophila* wing discs are not eliminated during development at least until pupal stage. After eclosion, *Drosophila* wings are filled with hemocytes[32] that are strongly stained with SA-β-Gal, and the adult wings possess autofluorescence that is spectroscopically similar to SPiDER, which hampers our analysis on cellular senescence in the adult wings using SPiDER or X-gal staining (Figure S6A). Intriguingly, we found that Pnt-expressing cell clusters still exist in the adult hinge radiuses (Figure S6B). Thus, although essential for normal tissue development, the fate and regulatory mechanisms of programmed senescent cells seem to be different between *Drosophila* and vertebrates.

Inhibition of programmed cell senescence led to loss of campaniform sensilla in dorsal and ventral radiuses. Interestingly, campaniform sensilla also exist in the adult legs and halteres,[21,33] and SA-β-gal-positive cells were also observed in the leg discs and haltere discs (Figure S1). The structure of campaniform sensilla includes a dome-shaped cuticular structure with a sensory neuron beneath it. When flies move or experience forces, the dome deforms, which in turn activates

Figure 3. Programmed cell senescence is required for campaniform sensilla development

(A and B) Wild-type wing discs were stained with SPiDER-βgal and anti-phospho-p44/42 MAPK (Erk1/2) (Thr202/Tyr204) antibody. The percentage of pERK-positive area (magenta) in SA-β-gal-activated clusters (white) was quantified in (B). Dorsal cells (n = 12), ventral cells (n = 12).

(C and D) Wild-type or *ci-Gal4>*Ras^{N17} wing discs were subjected to SA-β-gal assay. Arrowheads indicate DSCs. Intensity of senescent cells was measured with ImageJ and normalized with background. Data were collected as mean ± SE; wild type (n = 10), *ci>*Ras^{N17} (n = 6). Student's t test, $^{**}p < 0.01$.

(E) Wing disc expressing fly-FUCCI was stained with DAPI. PH, proximal hinge; DH, distal hinge.

(F) The location of senescent cells in the larval wing disc (left) and adult wing (right). A, anterior; P, posterior; D, dorsal; V, ventral.

(G–I) Campaniform sensilla (arrowheads) on dorsal and ventral radiuses of wild-type (G) and *ci>*Ras^{N17} (H) flies. The number of campaniform sensilla was counted and quantified (I). Data were collected as mean ± SE; n = 52 (wild-type dorsal radius), n = 42 (*ci>*Ras^{N17} dorsal radius), n = 29 (wild-type ventral radius), and n = 37 (*ci>*Ras^{N17} ventral radius). Student's t test, $^{***}p < 0.001$. Scale bars, 50 μm (A, C, E, G). See Table S1 for genotypes.

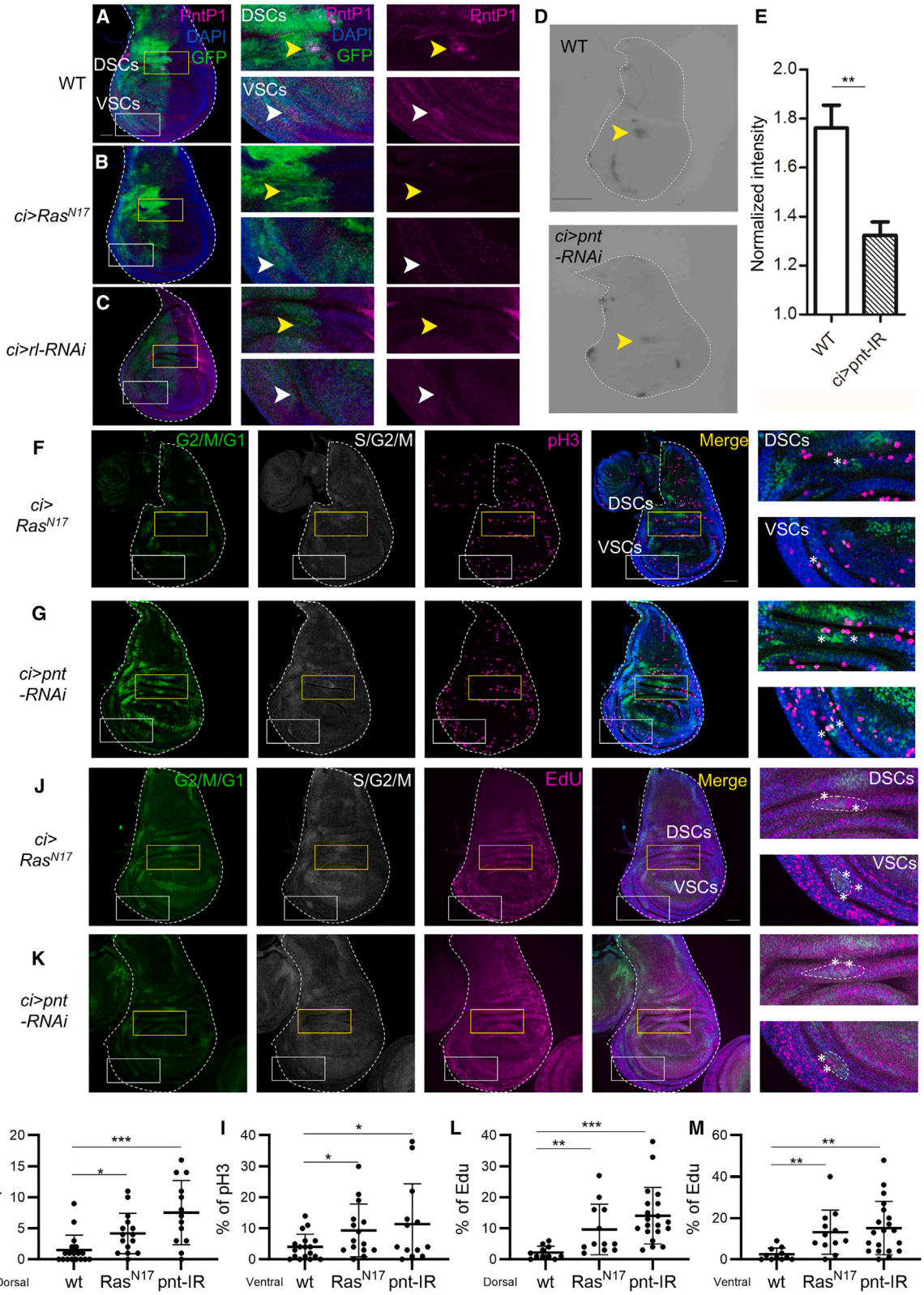

(legend on next page)

the sensory neuron. This allows flies to detect changes in mechanical forces, helping with balance, posture, and wing movement; thus flies can fly or walk. One specific morphological feature of campaniform sensilla compared to other mechanoreceptors such as macrochaetes or microchaetes is that they form caps instead of hairs. This could be a reason why they undergo senescence to generate a specific structure of the organ, possibly via tissue remodeling like programmed cell senescence in developing mice. Intriguingly, we found that programmed senescent cells upregulate an SASP factor Upd3, which may contribute to generating a specific structure of campaniform sensilla. A senolytic drug administration to flies may give us further information for the role of programmed cell senescence in different organs or tissues. Although our trial using a senolytic drug Navitoclax failed to eliminate DSCs and VSCs in the wing discs (data not shown), future studies with different senolytic drugs or conditions may provide further insights into the roles of developmentary programmed cellular senescence.

In mammals, programmed cell senescence and oncogene-induced senescence share a common signaling pathway for their induction.[34] Our analysis in *Drosophila* intriguingly found that programmed cell senescence is also triggered by Ras signaling, a common rigger of oncogene-induced senescence. Furthermore, a newly identified senescence mediator Zfh2 regulates both programmed cell senescence and oncogene-induced senescence in *Drosophila*. Thus, our study not only identifies the evolutionary conservation of programmed cell senescence but also expands the mechanistic similarities between oncogene-induced senescence and programmed cell senescence, which would provide a better understanding for various senescence-related diseases in humans.

Limitations of the study

Our observations in developing Drosophila wing discs revealed that programmed cell senescence is induced by the Ras-Pnt-Zfh2 pathway, which contributes to the formation of a specific sensory organ campaniform sensilla in the adults. In the future study, detailed investigation should be performed to track senescent cells from developing larval wing discs to sensory organ development in the adult, which is currently hampered by technical limitations. It should also be addressed how programmed cell senescence contributes to the formation of campaniform sensilla.

RESOURCE AVAILABILITY

Lead contact

For additional information or requests for resources and reagents, please contact the lead contact, Tatsushi Igaki (igaki.tatsushi.4s@kyoto-u.ac.jp).

Materials availability

This study did not generate new unique reagents.

Data and code availability

- No original code was generated in this study.
- All data presented in this paper will be made available upon request to the lead contact.
- Additional information necessary for data reanalysis can be obtained from the lead contact upon request.

ACKNOWLEDGMENTS

The authors would like to acknowledge T. Ito for sharing unpublished data and K. Baba, M. Koijima, M. Tanaka, M. Matsuoka, and K. Gomi for technical support. We also thank D. Bohmann, the Bloomington *Drosophila* Stock Center (BDSC, Indiana, USA), the Vienna *Drosophila* Resource Center (VDRC, Vienna, Austria), and the *Drosophila* Genomics and Genetic Resources (DGGR, Kyoto Stock Center, Japan) for fly stocks. We also would like to express our thanks to all the members of the Igaki laboratory for their inspiring ideas. This work was funded by grants from the MEXT/JSPS KAKENHI (Grant Number 16K14606) to T.I., the Takeda Science Foundation to T.I., and Japan Agency for Medical Research and Development (Project for Elucidating and Controlling Mechanisms of Aging and Longevity, Grant Number 17938731) to T.I.

AUTHOR CONTRIBUTIONS

T.I., Y.Z., and M.Y. designed the experiments; M.Y. performed initial experiments to identify programmed cell senescence; Y.Z. conducted the rest of the experiments and analyzed the data with input from T.I.; Y.Z. and T.I. wrote the manuscript.

DECLARATION OF INTERESTS

The authors declare no competing interests.

STAR★METHODS

Detailed methods are provided in the online version of this paper and include the following:

- KEY RESOURCES TABLE
- EXPERIMENTAL MODEL AND SUBJECT DETAILS
  - Experimental model
- METHOD DETAILS
  - *Drosophila* culture conditions and stains

Figure 4. Ras signaling induces programmed cell senescence via Pnt

(A–C) *ci>GFP* (A), *ci>Ras^{N17}*(B), or *ci>rl-RNAi*(C) wing disc with *Pnt-lacZ* was stained with anti-β-gal antibody. Yellow and white arrowheads indicate senescent cells.

(D and E) Wild-type and *ci>pnt-RNAi* wing discs subjected to SA-β-gal assay. Arrowheads indicate SA-β-gal-activated clusters. Intensity of X-gal staining in senescent cells was measured with ImageJ and normalized with background (E). Data were collected as mean ± SE; wild type ($n = 6$), *ci>pnt-IR* ($n = 6$). Student's t test, $^{**}p < 0.01$.

(F–I) Wing discs expressing fly-FUCCI with *ci> Ras^{N17}* (F) or *ci>pnt-RNAi* (G) were stained with anti-pH3 antibody. Asterisks represent pH3-positive cells. The percentage of pH3-positive area (magenta) in FUCCI clusters (green and white) was quantified in (H, I). Data were collected as mean ± SE; wild-type dorsal ($n = 18$), *ci>Ras^{N17}* dorsal ($n = 15$), *ci>pnt-IR* dorsal ($n = 13$), wild-type ventral ($n = 18$), *ci>Ras^{N17}* ventral ($n = 15$), *ci>pnt-IR* ventral ($n = 13$); Student's t test, $^{*}p < 0.05$, $^{***}p < 0.001$.

(J–M) Wing discs expressing fly-FUCCI with *ci> Ras^{N17}* (J), or *ci>pnt-RNAi* (K) were stained with EdU incorporation. Asterisks represent EdU-positive cells. The percentage of EdU-positive area (magenta) in FUCCI clusters (green and white) was quantified in (L, M). Data were collected as mean ± SE; wild-type dorsal ($n = 11$), *ci>Ras^{N17}* dorsal ($n = 12$), *ci>pnt-IR* dorsal ($n = 20$), wild-type ventral ($n = 11$), *ci>Ras^{N17}* ventral ($n = 12$), *ci>pnt-IR* ventral ($n = 20$). Student's t test, $^{**}p < 0.01$, $^{***}p < 0.001$. Scale bars, 50 μm (A–C, F, G, J, K) or 100 μm (D). See Table S1 for genotypes.

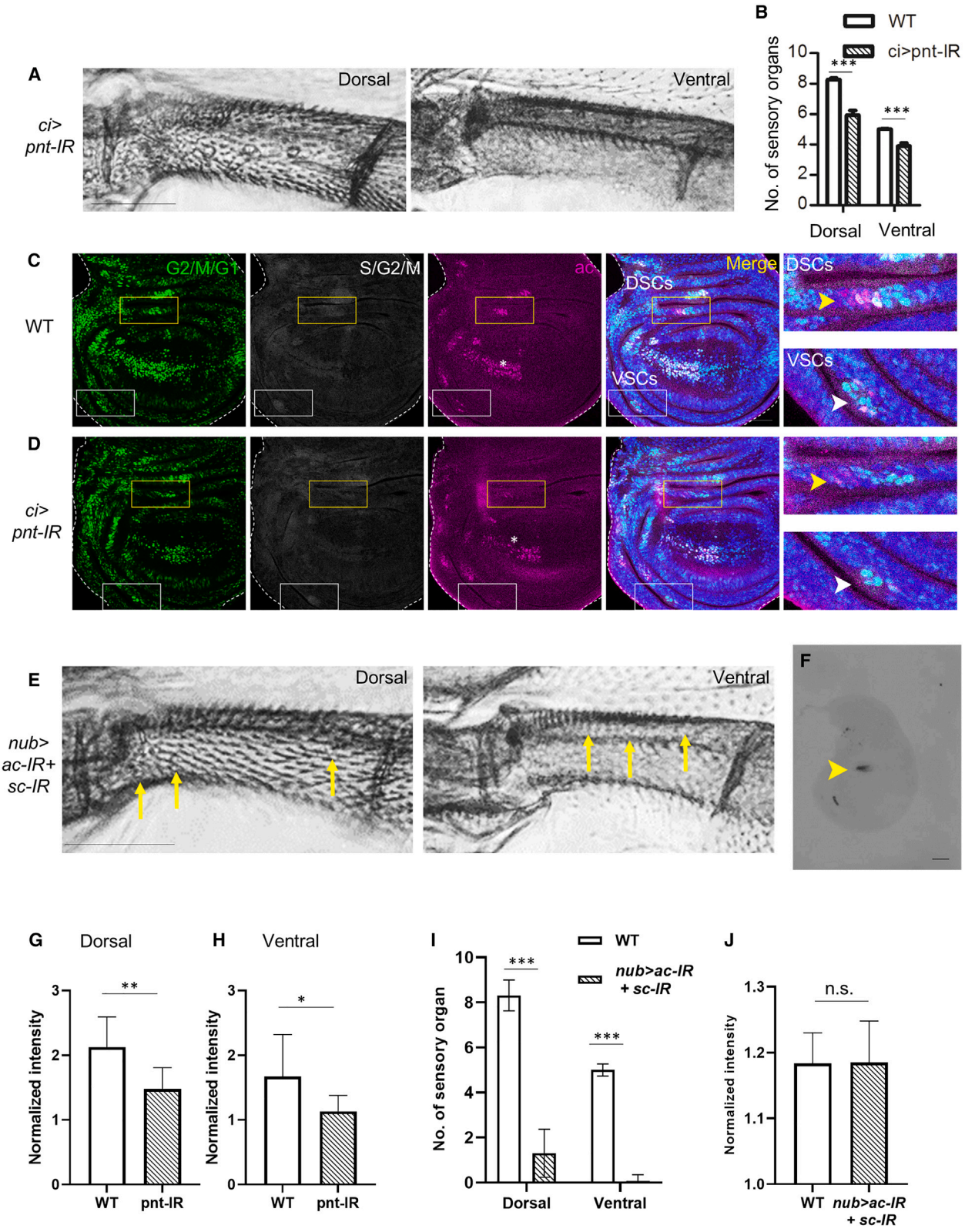

(legend on next page)

- SA-β-gal staining
- *Ex vivo* culturing of wing disc
- SPiDER-βgal staining
- Histology
- Wing image

- QUANTIFICATION AND STATISTICAL ANALYSIS

SUPPLEMENTAL INFORMATION

Supplemental information can be found online at https://doi.org/10.1016/j.isci.2025.112048.

Received: August 30, 2024
Revised: December 31, 2024
Accepted: February 13, 2025
Published: February 17, 2025

REFERENCES

1. Campisi, J., and D'Adda Di Fagagna, F. (2007). Cellular senescence: When bad things happen to good cells. Nat. Rev. Mol. Cell Biol. *8*, 729–740.
2. Campisi, J. (2013). Aging, Cellular Senescence, and Cancer. Annu. Rev. Physiol. *75*, 685–705.
3. Rodier, F., and Campisi, J. (2011). Four faces of cellular senescence. J. Cell Biol. *192*, 547–556.
4. Courtois-Cox, S., Jones, S.L., and Cichowski, K. (2008). Many roads lead to oncogene-induced senescence. Oncogene *27*, 2801–2809. https://doi.org/10.1038/sj.onc.1210950.
5. Serrano, M., Lin, A.W., McCurrach, M.E., Beach, D., and Lowe, S.W. (1997). Oncogenic ras provokes premature cell senescence associated with accumulation of p53 and p16INK4a. Cell *88*, 593–602.
6. Bernadotte, A., Mikhelson, V.M., and Spivak, I.M. (2016). Markers of cellular senescence. Telomere shortening as a marker of cellular senescence. Aging *8*, 3–11. https://doi.org/10.18632/aging.100871.
7. Jurk, D., Wilson, C., Passos, J.F., Oakley, F., Correia-Melo, C., Greaves, L., Saretzki, G., Fox, C., Lawless, C., Anderson, R., et al. (2014). Chronic inflammation induces telomere dysfunction and accelerates ageing in mice. Nat. Commun. *2*, 4172. https://doi.org/10.1038/ncomms5172.
8. Brandl, A., Meyer, M., Bechmann, V., Nerlich, M., and Angele, P. (2011). Oxidative stress induces senescence in human mesenchymal stem cells. Exp. Cell Res. *317*, 1541–1547.
9. Kuilman, T., Michaloglou, C., Mooi, W.J., and Peeper, D.S. (2010). The essence of senescence. Genes Dev. *24*, 2463–2479.
10. Storer, M., Mas, A., Robert-Moreno, A., Pecoraro, M., Ortells, M.C., Di Giacomo, V., Yosef, R., Pilpel, N., Krizhanovsky, V., Sharpe, J., and Keyes, W.M. (2013). Senescence is a developmental mechanism that contributes to embryonic growth and patterning. Cell *155*, 1119–1130.
11. Muñoz-Espín, D., Muñoz-Espín, D., Cañamero, M., Maraver, A., Gómez-López, G., Contreras, J., Murillo-Cuesta, S., Rodríguez-Baeza, A., Varela-Nieto, I., Ruberte, J., et al. (2013). Programmed cell senescence during mammalian embryonic development. Cell *155*, 1104–1118.
12. Zhao, Y., Tyshkovskiy, A., Muñoz-Espín, D., Tian, X., Serrano, M., de Magalhaes, J.P., Nevo, E., Gladyshev, V.N., Seluanov, A., and Gorbunova, V. (2018). Naked mole rats can undergo developmental, oncogene-induced and DNA damage-induced cellular senescence. Proc. Natl. Acad. Sci. USA *115*, 1801–1806.
13. Nacher, V., Carretero, A., Navarro, M., Armengol, C., Llombart, C., Rodríguez, A., Herrero-Fresneda, I., Ayuso, E., and Ruberte, J. (2006). The quail mesonephros: A new model for renal senescence? J. Vasc. Res. *43*, 581–586.
14. Davaapil, H., Brockes, J.P., and Yun, M.H. (2017). Conserved and novel functions of programmed cellular senescence during vertebrate development. Development *144*, 106–114.
15. Nakamura, M., Ohsawa, S., and Igaki, T. (2014). Mitochondrial defects trigger proliferation of neighbouring cells via a senescence-associated secretory phenotype in Drosophila. Nat. Commun. *5*, 5264–5311.
16. Nakamura, Y., Mochida, A., Nagaya, T., Okuyama, S., Ogata, F., Choyke, P.L., and Kobayashi, H. (2017). A topically-sprayable, activatable fluorescent and retaining probe, SPiDER-βGal for detecting cancer: Advantages of anchoring to cellular proteins after activation. Oncotarget *8*, 39512–39521.
17. Aldaz, S., Escudero, L.M., and Freeman, M. (2010). Live imaging of Drosophila imaginal disc development. Proc. Natl. Acad. Sci. USA *107*, 14217–14222.
18. Classen, A., Aigouy, B., Giangrande, A. and Eaton, S. Imaging Drosophila Pupal Wing Morphogenesis. In Methods in Molecular Biology *420*, C. Dahmann, ed., Humana Press. https://doi.org/10.1007/978-1-59745-583-1_16.
19. Zielke, N., Korzelius, J., van Straaten, M., Bender, K., Schuhknecht, G.F.P., Dutta, D., Xiang, J., and Edgar, B.A. (2014). Fly-FUCCI: A Versatile Tool for Studying Cell Proliferation in Complex Tissues. Cell Rep. *7*, 588–598. https://doi.org/10.1016/j.celrep.2014.03.020.
20. Roch, F., Jiménez, G., and Casanova, J. EGFR (2002). Signalling Inhibits Cic-Dependent Repression. Development *129*, 993–1002. https://doi.org/10.1242/dev.129.4.993.
21. Cole, E.S., and Palka, J. (1982). The pattern of campaniform sensilla on the wing and haltere of Drosophila melanogaster and several of its homeotic mutants. J. Embryol. Exp. Morphol. *71*, 41–61.
22. Ohtani, N., Zebedee, Z., Huot, T.J., Stinson, J.A., Sugimoto, M., Ohashi, Y., Sharrocks, A.D., Peters, G., and Hara, E. (2001). Opposing effects of Ets and Id proteins on p16INK4a expression during cellular senescence. Nature *409*, 1067–1070.
23. Scholz, H., Deatrick, J., Klaes, A., and Klämbt, C. (1993). Genetic dissection of pointed, a Drosophila gene encoding two ETS-related proteins. Genetics *135*, 455–468.
24. Klambt, C. (1993). The Drosophila gene pointed encodes two ETS-like proteins which are involved in the development of the midline glial cells. Development *117*, 163–176.

Figure 5. Pnt acts upstream of the *ac-sc* complex in campaniform sensilla development

(A and B) Campaniform sensilla on dorsal and ventral radiuses of *ci>pnt-RNAi* fly (A). The number of campaniform sensilla was counted and quantified (B). Data were collected as mean ± SE; $n = 52$ (wild-type dorsal radius), $n = 14$ (*ci>pnt-RNAi* dorsal radius), $n = 29$ (wild-type ventral radius), and $n = 19$ (*ci>pnt-RNAi* ventral radius). Student's t test, $^{***}p < 0.001$.

(C and D) Wing discs expressing fly-FUCCI with ci>+ (C) or ci>pnt-RNAi (D) were stained with anti-Ac antibody. Yellow arrowheads indicate DSCs, and white arrowheads indicate VSCs. Intensity of Ac expression (magenta) in FUCCI clusters (green and white) of interest was measured and quantified (G, H). Data were collected as mean ± SE; wild-type dorsal ($n = 16$), ci>pnt-IR dorsal ($n = 9$), wild-type ventral ($n = 16$), ci>pnt-IR ventral ($n = 9$). Student's t test, $^{*}p < 0.05$, $^{**}p < 0.01$.

(E and F) Knockdown of both *ac* and *sc* leads to loss of campaniform sensilla in the adults (E), whereas SA-β-gal activity in the wing disc is not affected by *ac-sc* knockdown (F). Arrowheads indicate campaniform sensilla on dorsal or ventral radius and senescent cells in the wing disc. The number of campaniform sensilla was counted and quantified (I). Data were collected as mean ± SE; $n = 52$ (wild-type dorsal radius), $n = 23$ (*nub>ac-RNAi +sc-RNAi* dorsal radius), $n = 29$ (wild-type ventral radius), and $n = 25$ (*nub>ac-RNAi +sc-RNAi* ventral radius). Student's t test, $^{***}p < 0.001$. Intensity of X-gal staining in senescent cells was measured with ImageJ and normalized with background (J). Data were collected as mean ± SE; wild-type ($n = 6$), *nub>ac-RNAi +sc-RNAi* ($n = 4$) Student's t test, $p > 0.5$. Scale bars, 50μm (A, C–F). See Table S1 for genotypes.

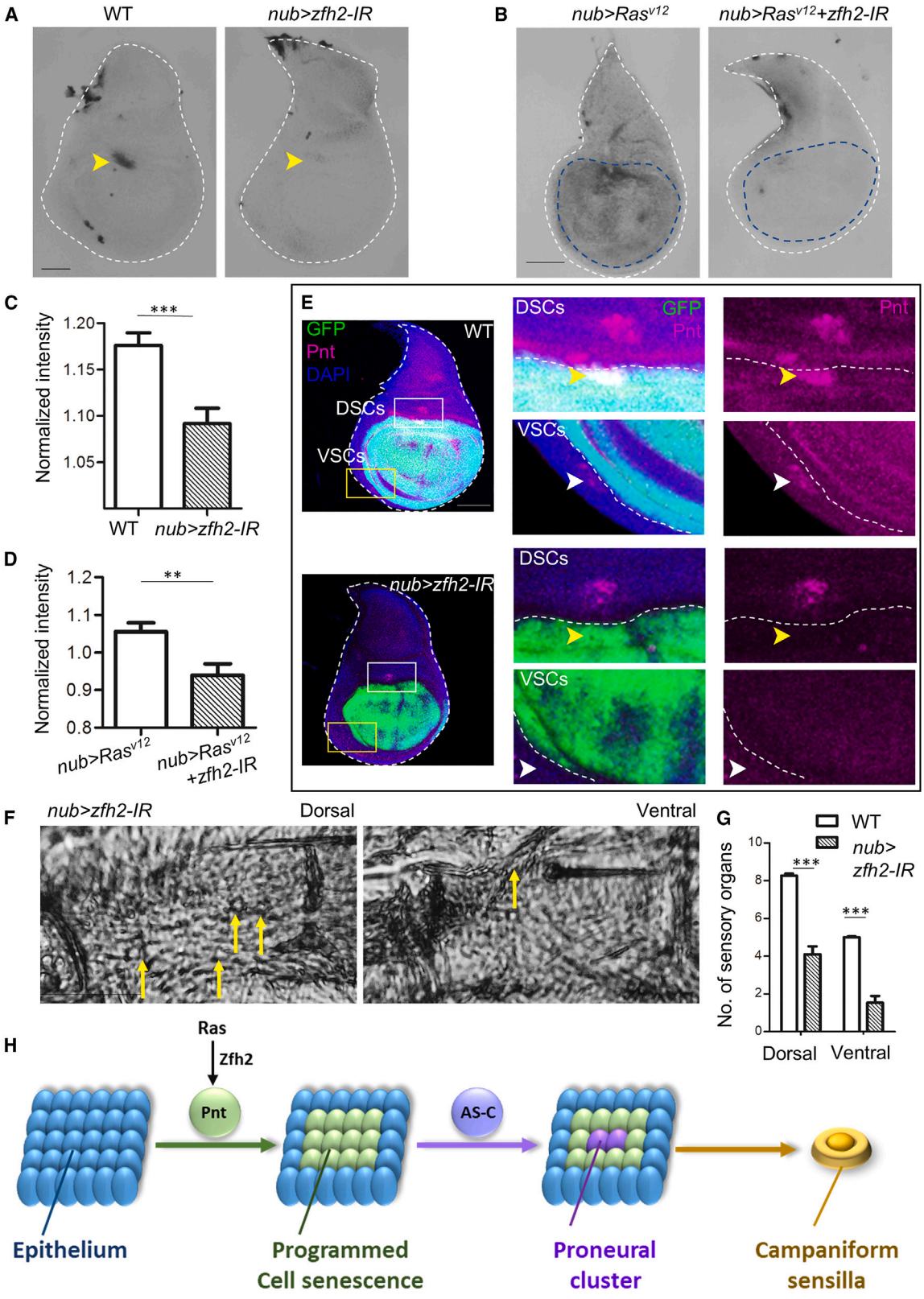

(legend on next page)

25. Shwartz, A., Yogev, S., Schejter, E.D., and Shilo, B.-Z. (2013). Sequential activation of ETS proteins provides a sustained transcriptional response to EGFR signaling. Development *140*, 2746–2754.

26. Ito, T., and Igaki, T. (2021). Yorkie drives Ras-induced tumor progression by microRNA-mediated inhibition of cellular senescence. Sci. Signal. *14*, eaaz3578.

27. Culí, J., Martín-Blanco, E., and Modolell, J. (2001). The EGF receptor and N signalling pathways act antagonistically in Drosophila mesothorax bristle patterning. Development *128*, 299–308.

28. Lage, P., Jan, Y.N., and Jarman, A.P. (1997). Requirement for EGF receptor signalling in neural recruitment during formation of Drosophila chordotonal sense organ clusters. Curr. Biol. *7*, 166–175.

29. Furman, D.P., and Bukharina, T.A. (2008). How Drosophila melanogaster Forms its Mechanoreceptors. Curr. Genom. *9*, 312–323.

30. Terriente, J., Perea, D., Suzanne, M., and Díaz-Benjumea, F.J. (2008). The Drosophila gene zfh2 is required to establish proximal-distal domains in the wing disc. Dev. Biol. *320*, 102–112.

31. Doggett, K., Turkel, N., Willoughby, L.F., Ellul, J., Murray, M.J., Richardson, H.E., and Brumby, A.M. (2015). BTB-zinc finger oncogenes are required for ras and notch-driven tumorigenesis in drosophila. PLoS One *10*, e0132987. https://doi.org/10.1371/journal.pone.0132987.

32. Kiger, J.A., Natzle, J.E., and Green, M.M. (2001). Hemocytes are essential for wing maturation in Drosophila melanogaster. Proc. Natl. Acad. Sci. USA *98*, 10190–10195.

33. Smith, S.A., and Shepherd, D. (1996). Central afferent projections of proprioceptive sensory neurons in Drosophila revealed with the enhancer-trap technique. J. Comp. Neurol. *364*, 311–323.

34. Muñoz-Espín, D., and Serrano, M. (2014). Cellular senescence: From physiology to pathology. Nat. Rev. Mol. Cell Biol. *15*, 482–496.

35. Harrison, D.A., McCoon, P.E., Binari, R., Gilman, M., and Perrimon, N. (1998). Drosophila unpaired encodes a secreted protein that activates the JAK signaling pathway. Genes Dev. *12*, 3252–3263.

36. Tseng, A.S.K., Tapon, N., Kanda, H., Cigizoglu, S., Edelmann, L., Pellock, B., White, K., and Hariharan, I.K. (2007). Capicua Regulates Cell Proliferation Downstream of the Receptor Tyrosine Kinase/Ras Signaling Pathway. Curr. Biol. *17*, 728–733.

37. Agaisse, H., Petersen, U.M., Boutros, M., Mathey-Prevot, B., and Perrimon, N. (2003). Signaling Role of Hemocytes in Drosophila JAK/STAT-Dependent Response to Septic Injury. Dev. Cell *5*, 441–450.

Figure 6. Zfh2-mediated Ras-Pnt signaling promotes campaniform sensilla development via *ac-sc*

(A) Wing disc from wild-type (left) or *nub>zfh2-RNAi* (right) larva was subjected to SA-β-gal assay. Arrowheads indicate dorsal senescent cell cluster. Intensity of X-gal staining in senescent cells was measured with ImageJ and normalized with background (C). Data were collected as mean ± SE; wild-type ($n = 9$), *nub>zfh2-RNAi* ($n = 12$). Student's t test, $^{***}p < 0.001$.

(B) Wing disc from *nub*>Ras^{V12} (left) or *nub*>Ras^{V12} + *zfh2-RNAi* (right) larva was subjected to SA-β-gal assay. Intensity of X-gal staining in senescent cells was measured with ImageJ and normalized with background (D). Data were collected as mean ± SE; *nub*>Ras^{V12} ($n = 6$), *nub*>Ras^{V12} + *zfh2-RNAi* ($n = 5$). Student's t test, $^{**}p < 0.01$.

(E) Wild-type or *nub>zfh2-RNAi* wing disc with *pnt-lacZ* was stained with anti-β-gal antibody. Yellow arrowheads indicate DSCs and VSCs.

(F and G) Campaniform sensilla (arrowheads) on dorsal and ventral radiuses of *nub>zfh2-RNAi* fly. The number of campaniform sensilla was counted and quantified (G). Data were collected as mean ± SE; $n = 52$ (wild-type dorsal radius), $n = 19$ (*nub>zfh2-RNAi* dorsal radius), $n = 29$ (wild-type ventral radius), and $n = 19$ (*nub>zfh2-RNAi* ventral radius). Student's t test, $^{***}p < 0.001$.

(H) Schematic representation of campaniform sensilla development via programmed cell senescence. Zfh2-mediated Ras-Pnt signaling induces programmed cell senescence, which promotes development of campaniform sensilla on dorsal and ventral radiuses via AS-C. Scale bars, 100 μm. See Table S1 for genotypes.

STAR★METHODS

KEY RESOURCES TABLE

REAGENT or RESOURCE	SOURCE	IDENTIFIER
Antibodies		
rabbit anti-Histone H3 (trimethyl K9) polyclonal	abcam	Cat# ab5819; RRID: AB_115065
chicken anti-β-galactosidase	abcam	Cat# ab9361; RRID: AB_307210
mouse anti-Dacapo,	DSHB	Cat# NP1; RRID: AB_10805540
rabbit anti-upd antibody	Harrison et al.[35]	N/A
mouse anti-mmp1	DSHB	Cat# 3A6B4; RRID: AB_579780
mouse anti-mmp1	DSHB	Cat# 5H7B11; RRID: AB_579779
mouse anti-mmp1	DSHB	Cat# 3B8D12; RRID: AB_579781
mouse anti-achaete	DSHB	Cat# anti-achaete; RRID: AB_528066
mouse anti-phospho histone H3	Cell Signaling Technology	Cat# 9701; RRID: AB_331535
guinea pig anti-Capicua polyclonal antibody	Tseng et al.[36]	N/A
Rabbit anti-phospho-p44/42 MAPK (Erk1/2) (Thr202/Tyr204)	Cell Signaling Technology	Cat# 4370; RRID: AB_2315112
Goat anti-rabbit secondary antibody, Alexa Fluor 488	Thermo Fisher Scientific	Cat# A-11070; RRID: AB_2534114
Goat anti-rabbit secondary antibody, Alexa Fluor 546	Thermo Fisher Scientific	Cat# A11035; RRID: AB_2534093
Goat anti-rabbit secondary antibody, Alexa Fluor 647	Thermo Fisher Scientific	Cat# A21246; RRID: AB_2535814
Goat anti-chick secondary antibody, Alexa Fluor 647	Thermo Fisher Scientific	Cat# A21449; RRID: AB_2535866
Goat anti-mouse secondary antibody, Alexa Fluor 647	Thermo Fisher Scientific	Cat# A-21237; RRID: AB_2535806
Goat anti-guinea pig secondary antibody, Alexa Fluor 546	Thermo Fisher Scientific	Cat# A-11074; RRID: AB_2534118
Chemicals, peptides, and recombinant proteins		
Shields and Sang M3 insect medium	Sigma-Aldrich	Cat# S3652-500ML
Alexa 546-conjugated phalloidin	Thermo Fisher Scientific	Cat# A22283
Slow Fade Gold antifade reagent with DAPI	Thermo Fisher Scientific	Cat# S36937
Critical commercial assays		
Senescent Cells Histochemical Staining Kit	Sigma-Aldrich	Cat# CS0030-1KT
Cellular Senescence Detection Kit SPiDER-βGal	Dojindo Molecular Technologies	Cat# 347-09181
Click-iT® EdU Imaging Kits	Thermo Fisher Scientific	Cat# C10340
Experimental models: organisms/strains		
Drosophila melanogaster: w1118	Bloomington Drosophila Stock Center	BDSC Cat#3605
Drosophila melanogaster: Ubi-GFP-E2F11-230 Ubi-mRFP-NLS-CyclinB1-260	Bloomington Drosophila Stock Center	BDSC Cat#55099
Drosophila melanogaster: *upd3-Gal4*	Agaisse et al.[37]	N/A
Drosophila melanogaster: *UAS-Ras^{N17}*	Kyoto Stock Center	DGGR Cat#107905
Drosophila melanogaster: *PntP1-lacZ^{HZ20}*	Shwartz et al.[25]	N/A
Drosophila melanogaster: *UAS-rl-RNAi* (III)	Bloomington Drosophila Stock Center	BDSC Cat# 34855
Drosophila melanogaster: *UAS-pnt-RNAi*	Vienna Drosophila Resource Center	VDRC Cat#v105390

(*Continued on next page*)

Continued

REAGENT or RESOURCE	SOURCE	IDENTIFIER
Drosophila melanogaster: *UAS-string*	Bloomington Drosophila Stock Center	BDSC Cat# 4777
Drosophila melanogaster: *UAS-ac-RNAi*	Bloomington Drosophila Stock Center	BDSC Cat# 42953
Drosophila melanogaster: *UAS-sc-RNAi*	Bloomington Drosophila Stock Center	BDSC Cat# 26206
Drosophila melanogaster: *UAS-zfh2-RNAi*	Bloomington Drosophila Stock Center	BDSC Cat# 50643
Software and algorithms		
Leica LAS AF software	Leica Microsystems	http://www.leica-microsystems.com/products/microscope-software/
ImageJ Software	National Institute of Health, USA	https://imagej.nih.gov/ij/
Excel	Microsoft	https://products.office.com/en-gb/excel
GraphPad Prism	GraphPad	https://www.graphpad.com/
Other		
Digital Color Camera Leica DFC310 FX	Leica Microsystems	https://www.leica-microsystems.com/
Leica TCS SP8 microscope	Leica Microsystems	https://www.leica-microsystems.com/
Leica Inverted Microscope for Cell Culture DMi1	Leica Microsystems	https://www.leica-microsystems.com/
Coolpix p340	Nikon	https://www.nikon-image.com/

EXPERIMENTAL MODEL AND SUBJECT DETAILS

Experimental model

Drosophila melanogaster

Flies were maintained at 25°C with a standard cornmeal-yeast food, unless otherwise stated.

All experiment used larvae or adults of both sex except for Ras^{N17} experiment (only females), as *UAS-*Ras^{N17} transgene is located on the X chromosome.

Larvae were collected at wandering third instar larval stage except for age-related assays.

METHOD DETAILS

Drosophila culture conditions and stains

The following stocks were used: *w1118*, *Ubi-GFP-E2F11-230 Ubi-mRFP-NLS-CyclinB1-260 (III)* (BL 55099), *gstD-GFP (X)* (a gift from D. Bohmann), *upd3-Gal4 (II)* (a gift from H. Agaisse), *ci-Gal4 (II)*, *nub-Gal4 (II)*, *ap-Gal4 (II)*, *UAS-*Ras^{N17}*(X)* (Kyoto Stock Center), *UAS-rl-RNAi*$^{TRiP.HMS00173}$ (III), *UAS-*Ras^{V12}*(II)*, *UAS-zfh2-RNAi*$^{TRiP.HMC03043}$ *(III)*, *PntP1-lacZ*^{HZ20} (a gift from B. Shilo), *UAS-pnt-RNAi*$^{VDRC.v105390}$ *(II)*, *UAS-ac-RNAi*$^{TRiP.HMS02646}$*(II)*, *UAS-sc-RNAi*$^{TRiP.JF02104}$ *(III)*, *sca-Gal4 (II)* (BL6479), *pnt-Gal4* ^{NP112814} *(III)*.

SA-β-gal staining

Senescent Cells Histochemical Staining Kit (CS0030, Sigma-Aldrich) was used to detect SA-β-gal activity. Larvae were dissected in PBS and then fixed with PFA. After washing with PBS 3 times, larvae were incubated in the Staining Mixture for 7 days at 37°C. Images were taken with a stereomicroscope.

Ex vivo culturing of wing disc

L3 larvae were dissected and cultured in Shields and Sang M3 insect medium (Sigma) with 2% FBS, 0.5% penicillin-streptomycin and 0.1 μg/mL Ecdysone (dissolved with 10% isopropanol first) for 24h in room temperature.[17]

SPiDER-βgal staining

Cellular Senescence Detection Kit SPiDER-βGal (SG-03, Dojindo Molecular Technologies) was used to analyze SA-β-gal activity. After dissecting in PBS, larvae or pupae were fixed with PFA and washed with PBS, then incubated in SPiDER-βgal working solution for 1h at 37°C. Images were taken with a Leica SP8 confocal microscope (Leica).

Histology

Larval tissues were stained with standard immunohistochemical procedures using chick anti-β-galactosidase polyclonal antibody (Abcam, 1:500), rabbit anti-Histone H3 (trimethyl K9) polyclonal antibody (Abcam, 1:50), mouse anti-Dacapo (Developmental Studies Hybridoma Bank, 1:6, for 7 days), rabbit anti-upd antibody (a gift from D. Harrison, 1:500), mouse anti-mmp1 (DSHB, 1:100 from 1:1:10 cocktail of 3A6B4, 3B8D12 and 5H7B11), mouse anti-achaete antibody (Developmental Studies Hybridoma Bank, 1:500),

mouse anti-phospho histone H3 antibody (Cell Signaling, 1:50), Capicua polyclonal antibody (a gift from Iswar Hariharan, 1:300), Rabbit anti-phospho-p44/42 MAPK (Erk1/2) (Thr202/Tyr204) antibody (Cell Signaling, 1:50), rat anti-Pnt antibody (1:10) or Alexa 546-conjugated phalloidin (Molecular Probes, 1:50) and were mounted with DAPI-containing SlowFade Gold Antifade Reagent (Molecular Probes). For EdU labeling, larvae were dissected in Schneider's medium and incubated in 1x EdU solution (Click-iT EdU Imaging Kits; Thermo Fisher Scientific C10340) for 10 min. After fixation and washing, tissues were incubated in EdU cocktail for 30 min and were mounted as described above. Images were taken with a Leica SP8 confocal microscope (Leica).

Wing image

Adult flies were incubated in a glycerol/ethanol mixture (1:1) for 1 day. Then wings were dissected from adult files then mounted with the glycerol/ethanol mixture and imaged with microscope.

QUANTIFICATION AND STATISTICAL ANALYSIS

The percentage of antibody staining/fluorescence marker-positive cells in SA-β-gal-elevated clusters was calculated in each disc by dividing the marker-positive area by SA-β-gal-elevated area.

The intensity of Tri-methylated H3K9 was quantified in individual nuclei, which was visualized by DAPI staining, and was normalized to the corresponding DAPI intensity.

Cell sizes were measured by ImageJ based on the outline of phalloidin staining.

The normalization of SA-β-gal intensity was conducted by dividing the intensity of senescence markers by the background intensity.

The number of campaniform sensilla was counted and was compared with the mean number of campaniform sensilla on wild-type wings.

The percentage of antibody staining/fluorescence marker-positive cells in senescent clusters was calculated in each disc by dividing the marker-positive area by FUCCI GFP and RFP-positive area.

Data were analyzed using Student's t test for single comparisons. Bar graphs represent the mean ± SE. All n values correspond to biological replicates. Statistical significance is indicated as follows: $^{***}p < 0.001$, $^{**}p < 0.01$, $^{*}p < 0.05$, and n.s. (not significant) for $p > 0.05$.